Collective resonances in carbon nanotubes

B. Vasvári
Department of Theoretical Physics, Technical University of Budapest, Budafoki ut 8, P.O. Box 112, Budapest H-1111, Hungary
(Received 18 October 1996)

A theory is presented to study the plasma oscillations of the full $\sigma+\pi$ electron system of carbon nanotubes. Cylindrical charge density was supposed to represent the electron distribution within the shells of the tubule and an integral equation is derived for the perturbation caused by an external electric field. From the solution of this equation the dynamical dipole polarizability is calculated in the energy range above 10 eV. For single-shell nanotubes a double-peaked spectrum resulted resembling the slow tangential and the fast radial dipole active mode of a classical spherical shell of finite width. The peak positions are around 17 and 22 eV for the smallest tubule radius and with increasing radius the low-energy peak shifts to a lower energy, the high-energy peak to a higher energy. For multishell nanotubes a strong shell-shell interaction is found, as a result of which the double-peaked structure of the innermost shell will be the dominant part in the imaginary part of the polarizability. With increasing shell number the low-energy peak shifts to a higher energy, the high-energy peak to lower energy; this is just the opposite tendency found in the radius dependence. For a large enough shell number the two peaks coincide at about 19 eV, and this value is independent of the radius of the innermost shell. Although the numbers mentioned may vary within 3–4 eV depending on the parameters of our models, the tendencies are in overall agreement with the existing electron energy loss spectroscopy measurements and with other theoretical predictions. [S0163-1829(97)03308-0]

I. INTRODUCTION

There is considerable research activity to clarify the physical properties of the recently discovered multishell, coaxial carbon nanotubes,[1–3] and the single-shell carbon tubules[4] as well. Tight-binding calculations[5–9] and density functional theory[10] for isolated single-shell nanotubes and for microbundles of these tubules[11] confirm the early results, that graphitic nanotubes exhibit metallic, semimetallic, or semiconducting electronic properties depending on their radii and helicity. The interlayer interaction is found to be low in tight-binding calculations for bilayer and multilayer nanotubes.[12,13] The experimental verification of these results is an outstanding task, mainly because of the difficulties in controlling the fine structure, like helicity, radius, number of layers, etc., of the nanotubes.

Parallel to the effort of finding the one-particle spectrum there are investigations to understand the collective excitations of this new form of carbon clusters. Experimentally the electron energy loss spectroscopy (EELS) is a direct way to measure the spectrum of plasma oscillations. To our knowledge until now only measurements on multishell nanutubes are available. Kuzuo *et al.*[14] found π plasmons at 5.2 and 6.4 eV, $\sigma+\pi$ plasmons between 22.0 and 24.5 eV. They have used a relatively large beam spot, so they probably measured more nanotubes simultaneously. Ajayan *et al.*[15] have seen a broad plasmon peak at about 27 eV in bulk graphite, and a systematic shift of this peak with a decreasing number of nanotube layers down to 18 eV for the smallest number of shells. This was interpreted as the $\sigma+\pi$ plasmon. The π plasmon peak appeared only in the case of a larger shell number. The position of the $\sigma+\pi$ peak depends also on the diameter of the innermost tubule. This means that there are two parameters, the diameter of the tube, and the number of layers, which affect the energy loss spectrum. Although the beam diameter was also larger than the tube diameters, the loss was measured on individual multishell nanotubes. Bursil *et al.*[16] have used a narrow electron beam diameter (nanoprobe) as small as about 2 nm which is smaller than the tube diameter and found a broad plasmon peak at around 15 eV but only for thin tubes consisting of less than 12 layers. This was interpreted as a surface plasmon. For 17 and 20 layers they found a superposition of the 15 eV and the 24 eV peaks, and for 29 layers they found only the 24 eV peak, which was measured also in a graphite slab containing 50 sheets lying parallel to the incident electron beam. This 24 eV peak was interpreted as a bulk $\sigma+\pi$ plasmon of graphite. The measured EELS spectra also showed the π plasmon around 6 eV.

In the theoretical calculations for collective excitations the electron gas is supposed to be confined to the two-dimensional surface of one or more cylindrical surfaces. Lin and Shung[17] evaluated the dielectric function within the random phase approximation (RPA), the zeros of this function defining the plasmon modes. They have found uncoupled acoustic and optical plasmon branches for zero or nonzero angular momentum changes, respectively. For double layer nanotubes the coupling between the two layers lead to important modifications. In their recent paper Lin and Shung[18] and Lin *et al.*[19] replaced the two-dimensional confinement by a tight-binding model but only for the π electrons and the $\epsilon(\omega)$ dielectric function was calculated within the gradient approximation,[20] and within the RPA.[19] The EELS defined as $\mathrm{Im}[-1/\epsilon(\omega)]$ shows the dominant π plasmon peak at $2\gamma_0 \simeq 6$ eV, where γ_0 is the resonance integral in the tight-binding scheme. Sato *et al.*[21] also calculated, within the RPA, the dielectric function of an electron gas confined to the surface of a hollow cylinder and found steplike behavior and a broad peak in the imaginary part of $\epsilon(\omega)$, as well as a

dimensional crossover from two-dimensional to one-dimensional character with decreasing tubule radius. Longe and Bose[22] used the two-dimensional model with the RPA for single-shell tubules and a classical dynamical model for multishell tubules to calculate the dielectric function and the dispersion relations for the collective oscillations and found one acoustic and several optical branches. Huaxiang *et al.*[23] started from the tight-binding model for the one-electron spectrum and calculated the imaginary part, $\epsilon_2(\omega)$, of the dielectric function for polarizations parallel to the tubule axis. For single-shell tubules the $\epsilon_2(\omega)$, which is proportional to the photoabsorption coefficient, is very similar to the metallic and semiconducting geometries and shows a broad peak around 15 eV, but is rather different below 8.8 eV for the two types of microtubules. This may be the consequence of the fact that for small energies the dielectric function is influenced mainly by the single-particle excitations, and they are different for the metallic and the semiconducting tubules. Davids *et al.*[24] considered the π electrons on the surface of a single cylindrical shell as an interacting two-dimensional Fermi gas, and calculated the quasiparticle energy spectrum analytically within the Hartree-Fock approximation, and the density-density response function in the RPA in order to get the dielectric function, the plasmon dispersion relations, and the differential cross section for electron-electron scattering. Numerical result were given for the cross sections for tubules of two different radii. For the smallest tubule of radius ($R=0.35$ nm) they have got a large resonance at 8.0 eV and a much broader resonance around 24–25 eV, for a tubule of larger radius ($R=1.45$ nm) the low-energy resonance is absent and the high-energy resonance occurs around 22 eV. This is somewhat surprising because the model treated the π electrons only. Using a two-dimensional classical hydrodynamical model for single and multishell nanotubes Yannouleas *et al.*[25,26] found a dimensionality crossover from a characteristic one-dimensional plasmon behavior to a three-dimensional one as the number of graphitic sheets increased.

The aim of the present paper is to find further details for the collective motion of the electron system in nanotubes. We follow the formalism developed first by Mukhopadhyay and Lundqvist[27–29] (ML) for the inhomogeneous electron system and applied it for the C_{60} fullerenes by Östling *et al.*[30] In the ML theory one can separate the single particle and collective components of the excitations, therefore it is particularly suitable if someone is interested only in the plasma oscillations of the electron system. The ML theory leads to an integral equation for the perturbation of the electron density caused by an external field. The integral equation needs as input functions the electron density and its gradient of the unperturbed electron system. To calculate this data we introduced a simple model: the single-shell tubule is represented by a macroscopically long cylinder with finite thickness. The potential is a rectangular well: zero outside of the tubule and a (negative) constant inside. We call this model the rectangular potential model. In our earlier paper[31] this model was used to calculate the polarizability and the EELS data of fullerenes supposing a spherical rectangular potential well and got reasonable results for the plasmon excitations both in the gas and the solid phase of C_{60}. It turned out that the steplike electron density, which is zero outside and constant inside of the tubule walls produces very nearly the same plasmon spectrum as the density calculated from the spherical well model. Therefore we used this simpler electron density to calculate the polarizability for multishell nanotubes also.

The outline of this paper is the following. In Sec. II we first give a short summary of the ML theory (II A), then we present its application to cylindrical systems (II B). In Sec. III we introduce the simple rectangular potential well model (III A) to calculate an electron density and present numerical results for the polarizability of single-shell nanotubes. Using the steplike distribution for the shape of the electron density in Sec. III B a theory is developed and numerical results are given for plasma oscillations and for the polarizability of multishell nanotubes. In Sec. IV we compare our results with measured EELS data, and with other theoretical approaches and summarize the results.

II. PLASMA OSCILLATIONS IN CYLINDRICAL SYMMETRICAL SYSTEMS

A. Review of the Mukhopadhyay and Lundqvist theory

The use of the ML theory[27–29] is advantageous if someone is interested only in the collective oscillations of an inhomogeneous electron system, since it provides a way to separate the individual and collective components of the excitations. Here we are giving a short summary of the ML theory.

Consider an electron system characterized by its density operator $\hat{\rho}(\mathbf{r},t)$. Suppose that an external potential, $V_{\text{ext}}(\mathbf{r},t)$ is applied to the system, and as a result of it an extra charge density, $\rho_1(\mathbf{r},t)$, is induced. In the linear response theory $\rho_1(\mathbf{r},t)$ and $V_{\text{ext}}(\mathbf{r},t)$ are related by the equation

$$\rho_1(\mathbf{r},t)=\int \mathbf{d}^3\mathbf{r}'dt'H(\mathbf{r},\mathbf{r}',t-t')V_{\text{ext}}(\mathbf{r}',t'), \qquad (1)$$

where the retarded density-density response function $H(\mathbf{r},\mathbf{r}',t-t')$ is given in the terms of the density operator

$$H(\mathbf{r},\mathbf{r}',t-t')=-i\Theta(t-t')\langle[\hat{\rho}(\mathbf{r},\mathbf{t}),\hat{\rho}(\mathbf{r}',\mathbf{t}')]\rangle. \qquad (2)$$

Here $\Theta(t)$ is the Heaviside step function, $\langle\ \rangle$ means the statistical average and $\hbar=1$ is in this chapter.

The induced $\rho_1(\mathbf{r},t)$ charge density produces an extra potential within the electron system, so the effective potential is given by

$$V_{\text{eff}}(\mathbf{r},t)=\int \mathbf{d}^3\mathbf{r}'v(\mathbf{r},\mathbf{r}')\rho_1(\mathbf{r}',t)+V_{\text{ext}}(\mathbf{r}',t), \qquad (3)$$

where $v(\mathbf{r},\mathbf{r}')=e^2/|\mathbf{r}-\mathbf{r}'|$ is the Coulomb potential. The response to the effective potential is described by

$$\rho_1(\mathbf{r},t)=\int \mathbf{d}^3\mathbf{r}'dt'h(\mathbf{r},\mathbf{r}',t-t')V_{\text{ext}}(\mathbf{r}',t'), \qquad (4)$$

with the retarded response function $h(\mathbf{r},\mathbf{r}',t-t')$ related to H by the equation $H=h+hvH$. In lowest order h is given in the terms of noninteracting system having the same ground-state density distribution function

$$h(\mathbf{r},\mathbf{r}',t-t')=-i\Theta(t-t')\langle[\hat{\rho}(\mathbf{r},t),\hat{\rho}(\mathbf{r}',t')]\rangle_0. \qquad (5)$$

This approach is equivalent to the random phase approximation. Differentiating Eq. (4) twice with respect to time t and using the equation of motion for $\hat{\rho}(\mathbf{r},t)$, ML proved that after Fourier transforming with respect to time, h can be separated into two parts $h=(h_i+h_c)/\omega^2$, where h_i depends only on the individual particle-hole excitations, and h_c only on the collective properties of the electron system:

$$h_i(\mathbf{r},\mathbf{r}',\omega)=-\sum_n \omega_n^2\left[\frac{\phi_n(\mathbf{r})\phi_n^*(\mathbf{r}')}{\omega+i\epsilon-\omega_n}-\frac{\phi_n(\mathbf{r}')\phi_n^*(\mathbf{r})}{\omega+i\epsilon+\omega_n}\right], \tag{6}$$

$$h_c(\mathbf{r},\mathbf{r}')=-\frac{1}{m}[\rho(\mathbf{r})\nabla_{\mathbf{r}}^2\delta(\mathbf{r}-\mathbf{r}')+\nabla\rho(\mathbf{r})\cdot\nabla_{\mathbf{r}}\delta(\mathbf{r}-\mathbf{r}')]. \tag{7}$$

Here $\omega_n=\epsilon_p-\epsilon_h$ is the particle-hole excitation energy, and $\phi_n(\mathbf{r})=\psi_p^*(\mathbf{r})\psi_h(\mathbf{r})$ is the corresponding density amplitude in the noninteracting system. Since we are interested only in the collective behaviors of the carbon nanotubes the h_i individual components will be neglected. In this approximation the H response function satisfies the

$$[\omega^2-\omega_{\rm pl}^2(\mathbf{r})]H(\mathbf{r},\mathbf{r}',\omega) =-h_c(\mathbf{r},\mathbf{r}')-\frac{1}{m}\nabla_{\mathbf{r}}\rho(\mathbf{r})\cdot\nabla_{\mathbf{r}}\int \mathbf{d}^3\mathbf{r}''v(\mathbf{r}-\mathbf{r}'')H(\mathbf{r}'',\mathbf{r}',\omega) \tag{8}$$

integral equation where

$$\omega_{\rm pl}(\mathbf{r})=\sqrt{\frac{4\pi e^2\rho(\mathbf{r})}{m}} \tag{9}$$

is the local plasma frequency.

B. Plasma oscillations and polarizability in cylindrical systems

Let us suppose that the unperturbed charge density possesses a cylindrical symmetry, $\rho(\mathbf{r})=\rho(r)$, where (r,θ,z) are the cylindrical coordinates. We are interested now in the collective density oscillations of this system under the influence of a homogeneous external field perpendicular to the cylindrical axis; $V_{\rm ext}(\mathbf{r},\omega)=-exE(\omega)$ with $x=r\cos(\theta)$. The induced dipole momentum is

$$P(\omega)=e\int \mathbf{d}^3\mathbf{r}\, x\rho_1(\mathbf{r},\omega). \tag{10}$$

Using the Fourier transform of Eq. (1) and the definition $\alpha(\omega)=P(\omega)/E(\omega)$, we get for the dipolar polarizability

$$\alpha(\omega)=-e^2\int \mathbf{d}^3\mathbf{r}\,\mathbf{d}^3\mathbf{r}'xH(\mathbf{r},\mathbf{r}',\omega)x'. \tag{11}$$

To calculate $\alpha(\omega)$ we have to multiply Eq. (8) from the left-hand side by x, from the right-hand side by x' and integrate with respect to the variables $\mathbf{r}$ and $\mathbf{r}'$. Turning to the cylindrical coordinates and taking into account that the density $\rho(r)$ depends only on the radial variable r, one can get for the left-hand side of Eq. (8),

$$L_1=S\int r^2dr[\omega^2-\omega_{\rm pl}^2(r)]f(r), \tag{12}$$

where we have introduced

$$f(r)=-\frac{e^2}{S}\int_0^{2\pi}d\theta\,\cos(\theta)\int_0^S dz\int \mathbf{d}^3\mathbf{r}'H(\mathbf{r},\mathbf{r}',\omega)x', \tag{13}$$

with S for the length of the system along the cylindrical axis. In the terms of this $f(r)$ function the dipolar polarizability is given simply by

$$\alpha(\omega)=S\int r^2f(r)dr. \tag{14}$$

Similarly the first term of the right-hand side of Eq. (8) leads to

$$L_2=-\frac{S}{4}\int r^2\frac{d\omega_{\rm pl}^2(r)}{dr}\,dr. \tag{15}$$

To carry out a similar calculation for the second term of the right-hand side of Eq. (8) one needs the expansion of the Coulomb potential in cylindrical coordinates[32]

$$v(\mathbf{r},\mathbf{r}')=\frac{2e^2}{\pi}\sum_{m=-\infty}^{m=\infty}e^{im(\theta-\theta')} \times\int_0^\infty dk\,\cos[k(z-z')]I_m(kr_<)K_m(kr_>), \tag{16}$$

where $I_m(x)$ and $K_m(x)$ are the mth-order modified Bessel functions of the first and second kind, respectively, $r_<$ ($r_>$) are the smaller (larger) of r and r'. The main advantage of this expansion is that it makes the integral with respect to the variables θ and z calculable, leaving only the $m=\pm1$ term from the summation and leading to a Dirac-δ function in the k integral. As a result one can get from the second term of the right-hand side of Eq. (8)

$$L_3=-\frac{S}{4}\int r^2dr\,\frac{d\omega_{\rm pl}^2(r)}{dr}\int dr'K(r,r')f(r'). \tag{17}$$

Collecting the three terms together one arrives to an integral equation for the function $f(r)$ as follows:

$$[\omega^2-\omega_{\rm pl}^2(r)]f(r)=g(r)\left[1+\int dr'K(r,r')f(r')\right], \tag{18}$$

where

$$g(r)=-\frac{1}{4}\frac{d\omega_{\rm pl}^2(r)}{dr}, \tag{19}$$

and

$$K(r,r')=\begin{cases}-2\left(\dfrac{r'}{r}\right)^2 & \text{if } r'<r\\ 0 & \text{if } r=r'\\ 2 & \text{if } r'>r.\end{cases} \tag{20}$$

Equations (14) and (18)–(20) are the basic result of the ML theory for the collective motion of a cylindrical electron system. Supposing that the charge density, i.e., the local plasma frequency, $\omega_{\rm pl}^2(r)$, and its derivative with respect to the cylindrical radius r is given, the $f(r)$ solution provides the dipolar polarizability $\alpha(\omega)$ with the help of Eq. (14).

III. SIMPLE MODELS AND RESULTS

A. The rectangular potential well model for single-shell nanotubes

1. The electron density distribution

To get a physically realistic still numerically manageable electron density we apply a simple model, which is similar to the empty lattice model used in solid state physics to describe the electronic band structure of simple solids. We suppose that a nanotube can be represented by a long, hollow cylinder along the z axes of our coordinate system, with a finite thickness v, and with an inner radius R_1, and outer radius R_2, with $v=R_2-R_1$. The detailed geometrical structure can be described by starting from a monatomic sheet of graphite.[8] First choose an arbitrary lattice point as the origin, and then another one with lattice vector $\mathbf{R}=n_1\mathbf{a}_1+n_2\mathbf{a}_2$, where $\mathbf{a}_1$ and $\mathbf{a}_2$ are the primitive vectors of the two-dimensional hexagonal lattice. Next we roll the sheet so that the second lattice point is superimposed on the origin. This gives us the skeleton of a carbon nanotube. We are using the notations of White *et al.*,[8] hence $n_1\geqslant n_2\geqslant 0$. All the geometric parameters of the tubule can be given in terms of the integers n_1 and n_2. The radius of the tubule $R=d_0\sqrt{3}(n_1^2+n_2^2+n_1n_2)^{1/2}/2\pi$, so $R_1=R-v/2$ and $R_2=R+v/2$, where $d_0=0.142$ nm is the interatomic distance in the graphitic sheet. The length of the unit cell in the z direction is $S_0=3d_0(n_1^2+n_2^2+n_1n_2)^{1/2}/L$, the number of carbon atoms within this unit cell is $n_{\rm at}=4(n_1^2+n_2^2+n_1n_2)/L$. Here $L=N$, where N is the largest common divisor of n_1 and n_2, except if $(n_1-n_2)/3N$ is an integer, in that case $L=3N$.

Using the one-electron approximation to describe the electron density within the tubule we suppose that the potential is constant, $-U_0$, inside R_1 and R_2, and zero outside. The one-electron Schrödinger equation should be written in cylindrical coordinates and the wave function can be separated in the form

$$\psi(r,\theta,z)=R(r)e^{il\theta}e^{ikz}. \tag{21}$$

Due to the rotational symmetry of our tubule potential the angular momentum quantum number has the values $l=0,\pm1,\pm2,\ldots$. In the z direction we introduce Born-Karman periodic boundary conditions within a macroscopic length S of the tubule, leading to the quasicontinuous values of the wave number $k=(2\pi/S)n$, where $n=0,\pm1,\pm2,\ldots,\pm N$, and $S=NS_0$. The radial component of the wave function satisfies the equations for the one-particle energy E with $y=r\sqrt{\kappa^2+k^2}$, $\kappa^2=-(2m/\hbar^2)E$,

$$y^2\frac{d^2R}{dR^2}+y\frac{dR}{dy}-[y^2+l^2]R=0, \tag{22}$$

if r is outside the tubule, $r<R_1$ or $r>R_2$, and

$$y^2\frac{d^2R}{dR^2}+y\frac{dR}{dy}+[y^2-l^2]R=0, \tag{23}$$

with $y=r\sqrt{-U_0+\kappa^2+k^2}$, if r is inside the tubule, $R_1\leqslant r\leqslant R_2$. The regular solutions of these equations

$$R_l(y)=\begin{cases} A_lI_l(y) & \text{if } r\leqslant R_1 \\ B_lJ_l(y)+C_lY_l(y) & \text{if } R_1\leqslant r\leqslant R_2 \\ D_lK_l(y) & \text{if } R_2\leqslant r, \end{cases} \tag{24}$$

where $I_l(y)$ and $K_l(y)$ are, as earlier, the modified Bessel functions, $J_l(y)$ and $Y_l(y)$ are the mth order Bessel functions of the first and second kind, respectively. Prescribing the continuity conditions for $R(y)$ and for its derivatives at R_1 and R_2 one can get for the energies

$$E_{l,i}(k)=x_{l,i}+\frac{\hbar^2}{2m}k^2. \tag{25}$$

For each angular momentum quantum number an additional index i is necessary because the finite potential well may possesses one, two, or more eigensolutions depending on v and U_0 and l. In the case of zero width one should get $x_l=-U_0+\hbar^2l^2/2mR^2$ with no additional index. The energy spectrum (25) consists of one-dimensional parabolic energy bands, shifted by the l-dependent $x_{l,i}$ values. All the bands have their own Fermi momenta, $k_{Fl,i}=\sqrt{(2m/\hbar^2)(\epsilon_F-x_{l,i})}$. The ϵ_F Fermi energy is defined by

$$n_0=\frac{2}{\pi}\sum_{l,i}p_l(2m/\hbar^2)(\epsilon_F-x_{l,i}). \tag{26}$$

Here $n_0=n_{\rm at}n_{\rm el}/S_0$ is the number of electrons in a tubule of unit length, $n_{\rm el}$ is the number of electrons per carbon atoms constituting the tubule. The parameter, $p_l=1$ if $l=0$, and $p_l=2$ otherwise, corresponds to the degeneracy of the angular momentum quantum number l. The volume density of electrons, needed for the local plasmon frequency in Eq. (9), is given by

$$\rho(r)=\sum_{l,i}p_l\frac{k_{Fl,i}}{\pi^2}|R_{l,i}(r)|^2, \tag{27}$$

supposing that the $R_{l,i}(r)$ radial wave functions are normalized to unity.

2. Numerical results for single-shell tubules

Our model for a single-shell nanotube contains four parameters: First, the integers (n_1,n_2), which describe the geometry, then the width, v, and the depth, U_0, of the rectangular potential well, responsible for the physics of the tubule. In our subsequent treatment it is supposed that we have four electrons per carbon atoms, that is the full $\sigma+\pi$ electron system is considered. In a similar calculation[31] for the C_{60} molecule the width was chosen as $v=0.30$ nm. Requiring that the highest occupied orbital should reproduce the ionization energy (7.54 eV) of the fullerene molecule gave us $U_0=-30.0$ eV. To our knowledge, there are no measurements for the ionization energy in the case of carbon nanotubes, therefore we have used, somewhat arbitrarily, the same numerical values for v and U_0 in the calculations pre-

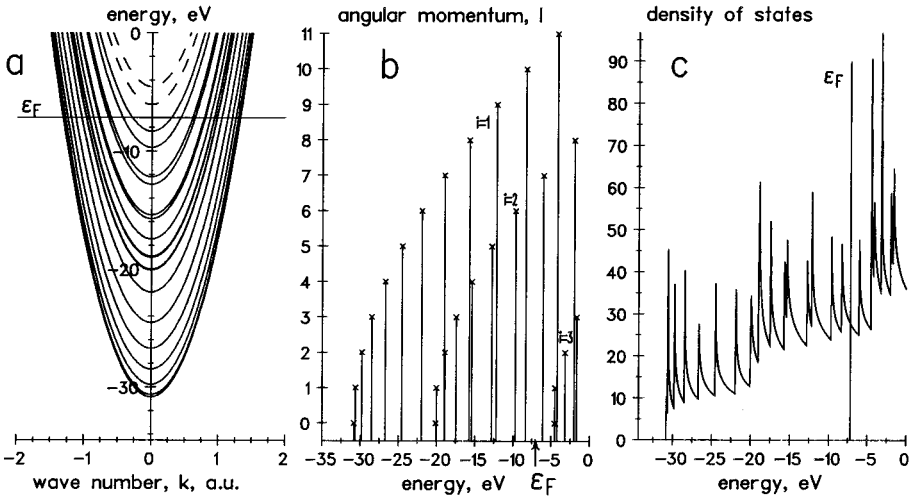

FIG. 1. The one-electron energy spectrum for the (10,0) tubule with radius $R=0.391$ nm in the rectangular cylindrical potential well model. The spectrum consists of coaxial parabolas shifted by the eigenenergies, $x_{l,i}$, of the potential well (a). The angular momentum quantum number l, and the index i are shown in diagram (b) for each of the eigenenergies. The density of states (c) exhibits singularities at $x_{l,i}$, due to the free motion of the electrons along the one-dimensional tubule axis. The $\epsilon_F=-7.18$ eV Fermi energy is determined by the number of atoms (40 for this tubule) and the number of electrons per atom (4 in our model). The width of the potential well, $v=2.5$ nm and the depth $U_0=-34.5$ eV.

sented in this paper. It turned out that our results are not very sensitive for the actual values of v and U_0, supposing that the Fermi energy remained around 7.0 eV.

The single-particle energy spectrum for the (10,0) tubule is shown in Fig. 1 together with the l angular momentum quantum numbers for the $x_{l,i}$ energy eigenvalues. It is remarkable that the $(l,x_{l,i})$ plot is nearly parabolic, as it should be in the case of the two-dimensional cylindrical model of zero width. The density of states curves show the one-dimensional type of singularities representing the free motion of the electrons along the z axis. In our simple model the nanotubes are always metallic, therefore the energy spectrum is not comparable with the results of tight binding or density functional calculations, which lead to a metallic, or semiconducting energy spectrum. Since we are interested now in the collective excitations of the $\sigma+\pi$ electron system with energies mainly above 10 eV, it is not critical whether the real system is metallic or semiconducting with an energy gap of 1–2 eV. What we need is the electron density, which readily can be calculated from the wave functions using Eq. (27). The results are shown in Fig. 2 for two tubules with radii $R=0.391$ and $R=1.174$ nm. One can see that the shape of the electron spatial distribution is almost independent of the radius of the single-shell tubules, therefore it is not necessary to recalculate them for larger radii. There is a small asymmetry between the increasing and the decreasing sides of the density profiles mainly for a smaller tubule radius, and a shallow minimum appears at the cylinder axis, because of the nodes of the wave functions for odd angular momentum quantum numbers.

To solve the integral equation (18) an imaginary part, $i\Gamma$, was attributed to the energy variable ω. For that reason a full complex arithmetic was used to get the complex solution $f(r)$, and the complex polarizability $\alpha(\omega)$. The numerical value of $\Gamma=1$ eV was supposed throughout the calculations reported in this paper.

The polarizabilties of single-shell nanotubes can be seen on Figs. 3 and 4. One can see a characteristic two-peak structure for the imaginary part of $\alpha(\omega)$, the intensity of the low-energy peak is higher than that of the high-energy peak. The width and the absolute magnitude of the peaks are dependent on the Γ artificial imaginary part of ω, therefore they have no physical meaning. Similar results were published for the C_{60} molecule by Lambin *et al.*[33] According to their model we may call the lower-energy peak the tangential, slow mode, and the higher-energy peak the radial, fast dipole active mode. For the smallest tubule radius the tan-

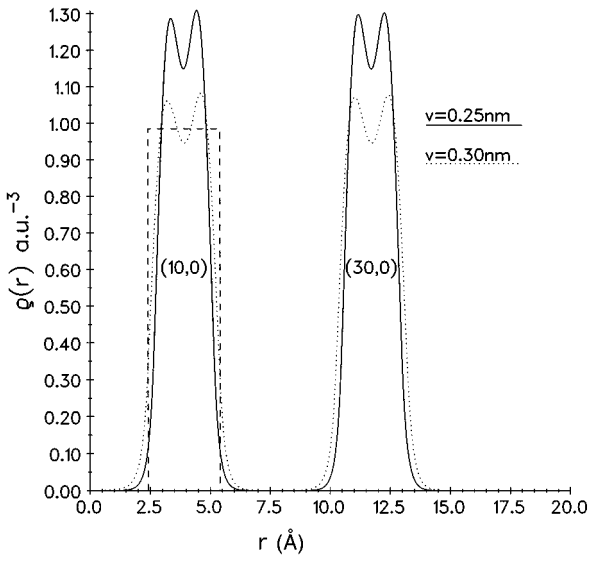

FIG. 2. Electron densities in atomic units for tubules (10,0) with radius $R=0.391$ nm and for (30,0) with radius $R=1.17$ nm. The parameters of the potential well $v=0.25$ nm, $U_0=-34.5$ eV (full line) and $v=0.30$ nm, $U_0=-30.0$ eV (dotted line). The dashed line on the tubule (10,0) shows the rectangular density profile used in Sec. III B.

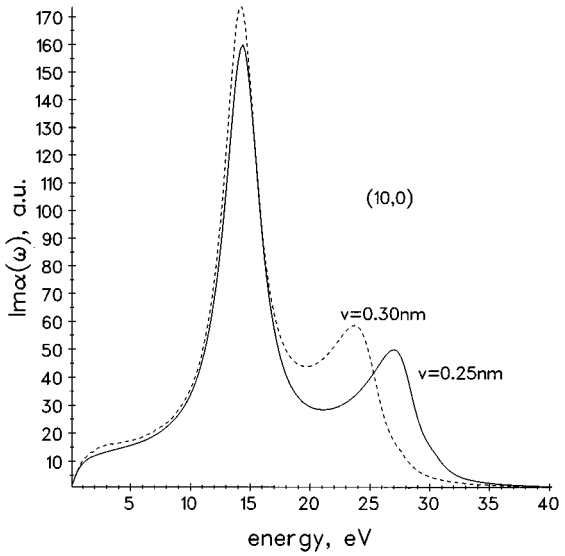

FIG. 3. Imaginary part of the polarizability of the tubule (10,0) for two sets of the potential parameters: $v=0.25$ nm, $U_0=-34.5$ eV (full line) and $v=0.30$ nm, $U_0=-30.0$ eV (dotted line).

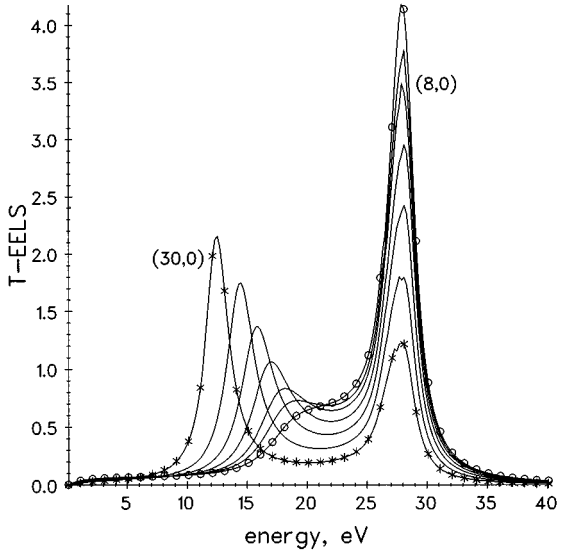

FIG. 5. The transmission electron energy loss spectrum for the bundles of nanotubes $(n,0)$, where $n=8$ (circles), $n=9,10,12,15,20$ (successive full lines), and $n=30$ (crosses).

gential peak is at about 17 eV, the radial one is at about 22 eV. With an increasing radius the position of the tangential component tends to a lower energy and that of the radial component to a higher energy (Fig. 4). For a fix radius the tangential component remains at the same energy, but the radial one shifts to somewhat higher energies with decreasing width of the potential well (Fig. 3).

Instead of a single nanotube, one may be interested in the properties of a bundle of tubules. We can imagine such a bundle as being made from single-shell nanotubes, with a parallel axis forming a hexagonal lattice. The perpendicular distance between two neighboring axes is $d=2R+b_0$, where R is the radius of a single tube, and b_0 is the smallest distance between two tubules. We may suppose that $b_0=0.342$ nm, which is the interlayer distance in solid graphite. The number density of nanotubes in the plane perpendicular to the tube axis is $n=(4/\sqrt{27})/d^2$. Neglecting the interaction between the individual nanotubes the complex dielectric function can be calculated from our polarizability as $\epsilon(\omega)=1+4\pi n\alpha(\omega)$. The transmission electron energy loss spectra, measured on the bundle of these nanotubes are proportional to $\mathrm{Im}(-1/\epsilon(\omega))$. The loss spectra are also double peaked, with the remarkable difference that the higher-energy peak at about 28 eV is independent of the tubule radius, while the position of the low-energy peak shifts to lower energies with an increasing radius (Fig. 5).

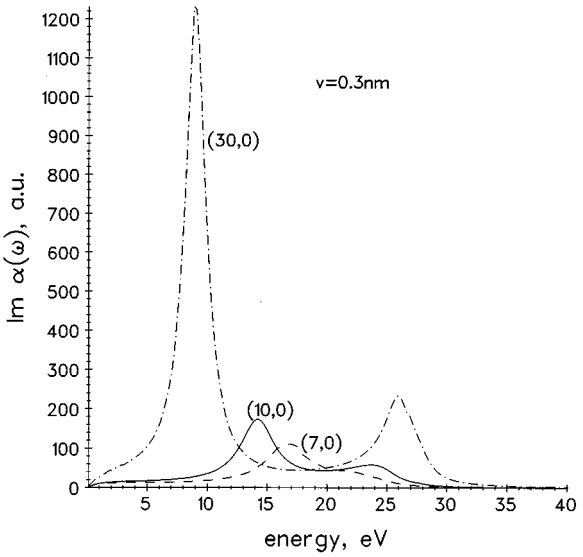

FIG. 4. Imaginary part of the polarizability of the tubules (7,0), (10,0), and (30,0) with radii 0.274, 0.391, and 1.174 nm, respectively. The potential well parameters here and in the following figures: $v=0.30$ nm, $U_0=-30.0$ eV.

B. Rectangular density distributions, multishell tubules

1. The dipole polarizability for multishell tubules

The generalization of the theory described in Sec. III A for multiple layer nanotubes is straightforward, but its numerical realization, especially the solution of the integral equation (18)–(20) is a formidable task. To simplify the treatment we introduce a further assumption to our model. The shape of the electron density distribution (Fig. 2) is approximated with a steplike function, which is zero outside the tubule and constant inside. We call this model the rectangular density model. This model was already successfully applied for the C_{60} molecule by Östling *et al.*[30] and Vasvári,[31] and for multishell carbon onions by Apell *et al.*[34] Suppose, that we have a multishell tubule with an N number of coaxial cylindrical shells, each having a radius R_i and the same thickness v. The squared local plasma frequency, which is proportional to the electron density is defined as

$$\omega_{\mathrm{pl}}^2(r)=\omega_0^2\sum_{i=1}^{N}\Theta(r-a_i)\Theta(b_i-r), \tag{28}$$

where $a_i = R_i - v/2$ and $b_i = R_i + v/2$, and $\Theta(r)$ is the Heaviside step function. The innermost tubule, its radius R_1, is defined by the pair of integers (n_1, n_2). For this tubule we calculated the electron density $n(r)$ as in the case of the single tubule using the same parameters v and U_0 as before. Then the parameter ω_0^2 was chosen by requiring that the area $v\omega_0^2$ should be equal to the area under the full local plasmon frequency curve on the r axis (see Fig. 2):

$$\omega_0^2 = (1/v)(4\pi e^2/m)\int_0^\infty n(r)dr. \tag{29}$$

The parameters v and ω_0^2 were the same for all the shells, each radius R_i was bigger than the previous one by $b_0 = 0.342$ nm. According to this model, the geometry of each multishell tubule is characterized by the integers for the innermost shell, (n_1, n_2), and the number of layers N, with the same charge density on each shell.

For the solution of the integral equation (18) we use the *ansatz*

$$f(r) = \sum_{i=1}^{N} [A_i \delta(r - a_i) + B_i \delta(r - b_i)]. \tag{30}$$

Substituting this form for $f(r)$ into Eq. (18) after a lengthy but straightforward algebra one can get a set of linear inhomogeneous equations for the coefficients A_i and B_i, $i = 1, \ldots, N$,

$$\sum_{j=1}^{N} \left\{ \left[\frac{\omega_0^2}{4} K(a_i, a_j) + \left(\omega^2 - \frac{\omega_0^2}{2} \right) \delta_{ij} \right] A_j + \frac{\omega_0^2}{4} K(a_i, b_j) B_j \right\} = -\frac{\omega_0^2}{4},$$

$$\sum_{j=1}^{N} \left\{ -\frac{\omega_0^2}{4} K(b_i, a_j) A_j + \left[-\frac{\omega_0^2}{4} K(b_i, b_j) + \left(\omega^2 - \frac{\omega_0^2}{2} \right) \delta_{ij} \right] B_j \right\} = \frac{\omega_0^2}{4}, \tag{31}$$

with the $K(r, r')$ function given by Eq. (20). The polarizability can be expressed in the terms of the coefficients A_i, B_i as follows:

$$\alpha(\omega) = \sum_{i=1}^{N} [A_i a_i^2 + B_i b_i^2]. \tag{32}$$

For a single-shell tubule, $N = 1$, these equations can be solved explicitly:

$$A_1 = -\frac{\omega_0^2}{4D(\omega)}\omega^2,$$

$$B_1 = \frac{\omega_0^2}{4D(\omega)}\left[\omega^2 - \frac{\omega_0^2}{2}\left(1 - \frac{a_1^2}{b_1^2} \right) \right], \tag{33}$$

where

$$D(\omega) = \left(\omega^2 - \frac{\omega_0^2}{2} \right)^2 - \frac{\omega_0^4}{4}\frac{a_1^2}{b_1^2} \tag{34}$$

is the determinant of the corresponding homogeneous equation. The zeros of this determinant give the eigenfrequencies of a single wall tubule

$$\omega_\pm^2 = \frac{\omega_0^2}{2}\left(1 \pm \frac{a_1}{b_1} \right), \tag{35}$$

the smaller being the tangential, the larger the radial dipole active mode. The polarizability

$$\alpha(\omega) = \frac{\omega_0^2}{4D(\omega)}\left(\omega^2 - \frac{\omega_0^2}{2} \right)(a_1^2 - b_1^2). \tag{36}$$

For the $\omega = 0$ static dipole polarizability this gives for a single-shell tubule of unit length $\alpha(0) = b_1^2/2$.

2. Numerical results for multishell tubules

The first question to be answered is how do the two solutions for the single wall nanotube agree with each other? Figure 6 shows the comparison of the (10,0) nanotube with a smaller radius ($R = 0.39$ nm) and of the (30,0) nanotube with a larger one ($R = 1.17$ nm). One can see the overall similarity of the two approaches, although there are some differences also, mainly in the relative height of the peaks and somewhat in the positions, too. These deviations are the consequences of the differences in the shape of the electron density distributions, which is a bit asymmetrical in the case of the rectangular potential model, and completely symmetrical in the case of the rectangular density model. The qualitative results of the two models are the same. For that reason, we may use the simplified rectangular density model to calculate some characteristic tendencies of the multishell nanotubes.

First we have to find out the intensity of the shell-shell interaction in the multishell tubules. For that reason we have calculated the imaginary part of the polarizability first for two separate single-shell tubules of (10,0) and (50,0) with a large difference between their radii, $R_1 = 0.391$ and $R_2 = 1.96$ nm, respectively, [dashed and dotted lines of Fig. 7(b)], next for a system of a double-shell nanotube with the same shell radii. The shell-shell interaction is represented in our basic equation (31) by the kernel $K(r, r')$ when one of its variables is from one shell and the other variable is from the other shell. If we artificially switch off this term from Eq. (31) then we get simply the sum of the two polarizabilities [dashed-dotted line Fig. 7(b)]. Switching on the interaction,

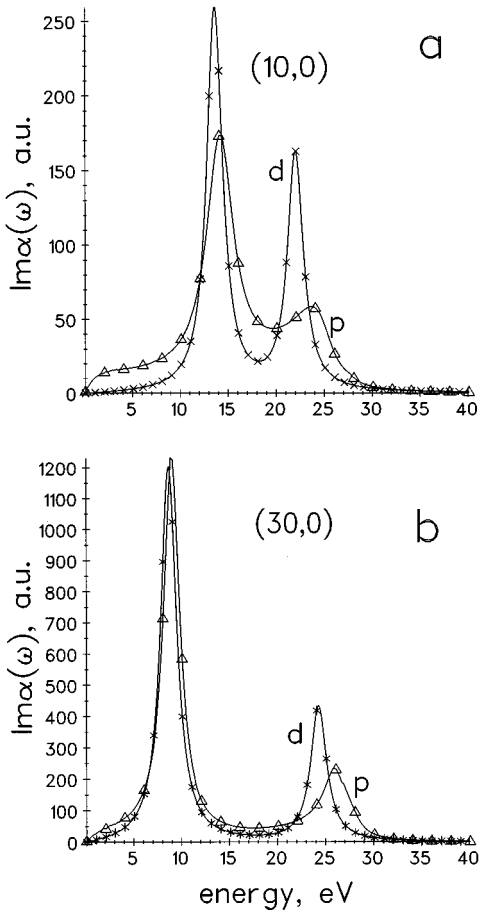

FIG. 6. Comparison of the polarizabilities calculated from the rectangular potential (p) model and the rectangular density (d) model for the tubules (10,0) (a), and (30,0) (b).

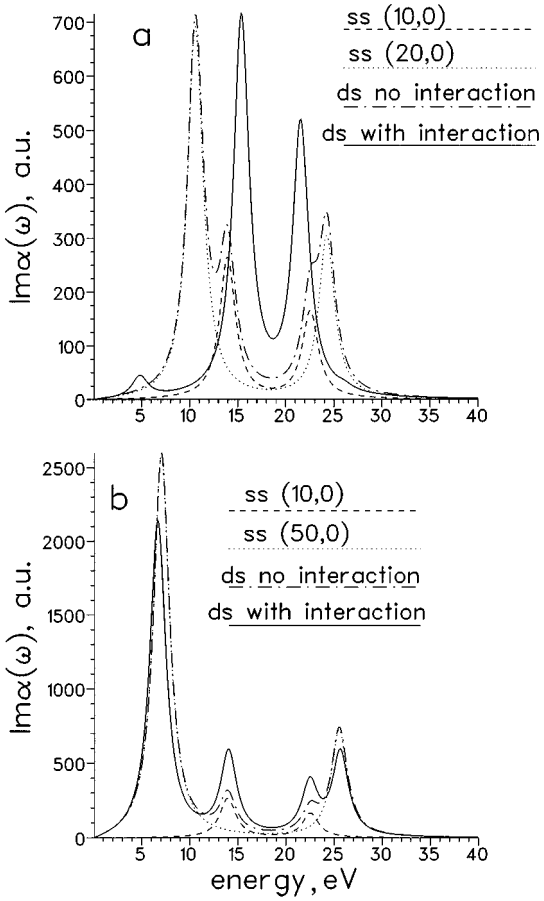

FIG. 7. The effect of the shell-shell interaction. The imaginary part of the polarizability for a double-shell nanotube, (a) the shell is the (10,0) type with radius 0.391 nm, the outer shell is the (20,0) type with radius 0.782 nm. Dotted and dashed lines are the polarizabilities of the single-shell (ss) nanotubes (10,0) and (20,0), respectively. The dash-dotted line is the double-shell (ds) polarizability with the shell-shell interaction switched off, the full line is the ds polarizability with the interaction involved. (b) The same with the tubules (10,0) and (50,0) with outer radius 1.958 nm. For such a large distance between the two shells their interaction is reduced, but still not negligible.

one can see that the effect is small, but not negligible still in this case of large distances between the two shells [full line of Fig. 7(b)]. There is a small shift downward on the energy scale for the lower-energy peak position of the outer tubule, while the higher-energy peak practically remains at the same position. There is, however, a considerable decrease of the outer peak intensities and an increase of the inner intensities as an effect of interaction. Figure 7(a) shows the same for tubules (10,0) and (20,0), $R_2 = 0.782$ nm, with a smaller difference in the shell radii. One can see a strong effect of the shell-shell interaction, a larger shift in the peak positions, and an almost complete disappearing of the peaks of the outer shell, and a considerable increase of the intensities belonging to the inner shell. To see the details of these dramatic changes Fig. 8 shows this tendency for gradually decreasing the distances of the tubule shells from $6b_0$ to $b_0 = 0.34$ nm, which is the distance of the carbon sheets in solid graphite. Practically the peaks corresponding to the outer shell disappeared, and the positions of the two peaks corresponding to the inner shell shifted towards each other as a consequence of the shell-shell interaction. The same tendency can be discovered for a three-shell nanotube also (Fig. 9). Hence we have to realize that the interaction between the tubule shells is far from being negligible.

The same effect is manifested when the number of sheets of a multishell nanotube changes. Figure 10 shows the polarizability from the single-shell tubule to shell number $N = 25$. The innermost tubule is the (10,0) tube with radius $R = 0.39$ nm with two peaks, one around 14.0 eV and another one around 22.5 eV. Increasing the number of shells only these two peaks remain, getting closer and closer to each other, forming a single peak around 19.0 eV for the shell number $N = 20$. We obtained the same trend for the other radius for the innermost tubule, with the difference that with an increasing radius the two peaks of the innermost tubule became more separated (Fig. 11), therefore they will form a single peak only for larger shell numbers. For the biggest innermost tubule investigated in this paper, (50,0), with radius $R = 1.96$ nm, the two peaks are around 7.1 eV and 25.5 eV for a single-shell tubule, and they approach each other as close as 18.1 eV and 19.3 eV for a multishell tubule with a

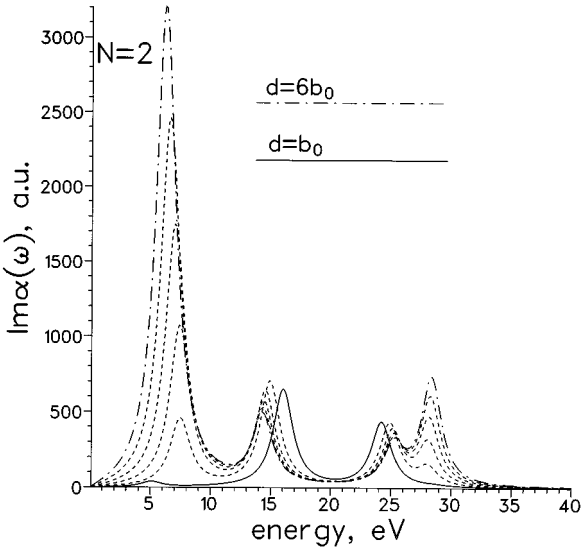

FIG. 8. Two-shell tubule with decreasing shell-shell distance. Dashed-dotted line is for distance $d=6b_0$, where $b_0=0.342$ nm is the interplanar distance in solid graphite. Subsequent dotted lines correspond to $d=5b_0$, $d=4b_0$, $d=3b_0$, $d=2b_0$; full line: $d=b_0$.

shell number $N=100$. This looks like a single peak for the case of a spectroscopic resolution less than 1–1.5 eV.

IV. DISCUSSION AND SUMMARY

First of all we have to emphasize that the ML theory that we have applied for carbon nanotubes neglects the single-particle contributions to the polarizability, therefore, our results are definitely not applicable in the energy range below, say, 5–7 eV, where the electron-hole excitations play the dominant role. Also, the broadening of the plasmon peaks are the consequence of the single-particle excitations, therefore, the width of the peaks, which is produced in our calculations by the artificially chosen imaginary part of the ω energy, does not bear on physical meaning. Other reason of

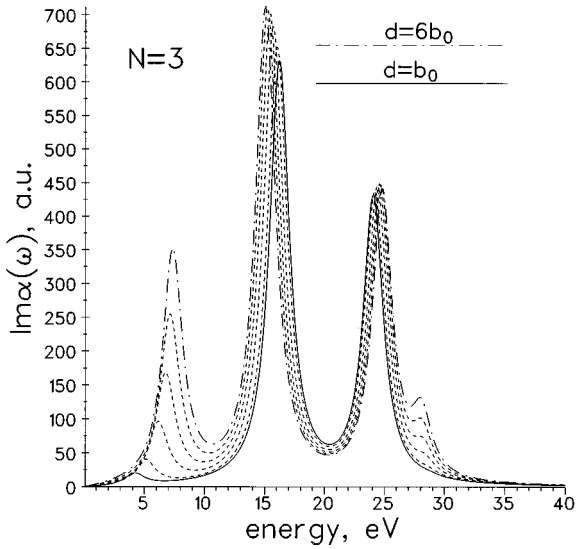

FIG. 9. The same as Fig. 8 but for a three-shell tubule.

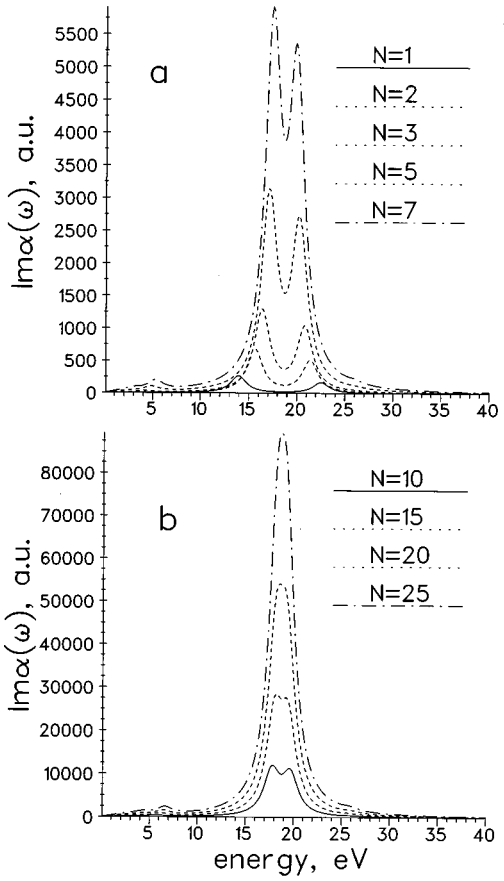

FIG. 10. Shell-number dependence of the polarizability. The innermost tubule [$N=1$, full line on (a)] is of the (10,0) type, the subsequent shells follow to a distance $b_0=0.342$ nm from the previous one. The subsequent curves on diagrams (a) and (b) correspond to different shell numbers N, as indicated on the figure.

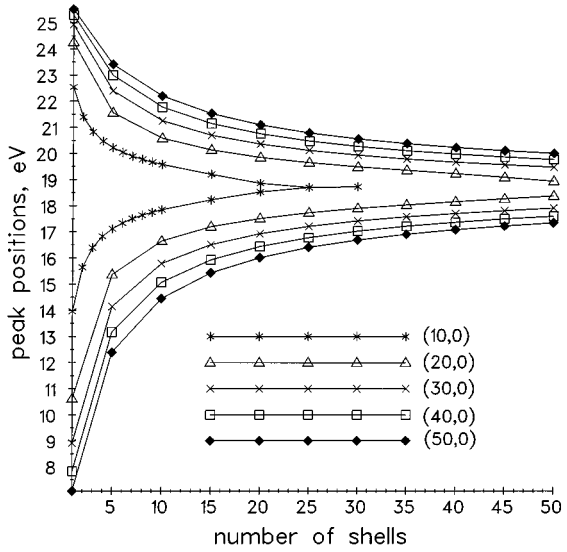

FIG. 11. Shell-number dependence of peak positions for the imaginary part of the polarizability for nanotubes with various innermost tubules of type (10,0), . . . ,(50,0).

the broadening of the experimental peaks may be the dispersion of the plasmon frequencies. It may occur that a momentum transfer is also present in the experimental circumstances, and our calculations correspond to the case of zero momentum transfer. It should also be noticed that we have calculated only the dipole excitations ($l=1$), while in the actual situation multipole transitions may also be present, giving rise to further broadening of the spectrum. We have to mention that in deriving our formulas we suppose the excitations are induced by a homogeneous electric field, perpendicular to the cylinder axis. This condition is usually fulfilled in optical measurements, but it may be questionable in EELS, if the diameter of the electron beam is less than or comparable to the tube diameter. This was the case in the experiments of Bursill *et al.*[16] For all of these reasons we do not expect a quantitative agreement between our calculated spectrum and the presently available experimental data, but we do expect that our results are predictive for the measurements of optical absorption coefficient on individual nanotubes of either single- or multishell type, and at least the peak positions of the EELS results can be interpreted in the terms of our model.

To our knowledge there were no optical measurements on nanotubes until now. In EELS experiments the number of shells and the diameter of the innermost tubule are not always indicated in the published results. The width of the measured EELS peaks is as large as 8–10 eV, and they do not exhibit a double-peak character. We expect that in the case of large innermost radius and small shell numbers there should be a double-peak spectrum in optical and EELS measurements also. The measured EELS peak positions are dependent both on the number of shells and the diameter of the nanotubes.[14–16] There is a single broad peak around 15–18 eV for a smaller (less than ~ 12) shell number and a shift of this peak to 22–27 eV with increasing shell number. In our calculated $\mathrm{Im}\alpha(\omega)$ functions the small-energy peak always has a higher intensity than the high-energy one, especially for the more precise rectangular potential well model (see Figs. 3, 4, 6). In the case of the nanotubes with a (10,0)-type innermost tube the calculated low-energy peak position increases from 14 eV for a single-shell tubule to 18.7 eV for a large shell number. From shell number 15 the difference between the positions of the low- and large-energy peaks is less than 1 eV, and remains constant at about 19 eV, independently of the radius of the innermost shell (Fig. 11). If we attribute our low-energy dipole active mode to the measured EELS spectrum, then the general tendencies of the measured spectrum are in agreement with our calculated data.

Regarding the published theoretical results we can compare our results with the calculations of Apell *et al.*[34] for the multishell fullerene onions. We followed nearly the same model for the cylindrical carbon nanotubes as they have used for the spherical C_{60}-based multishell fullerene molecules. The results of the two calculations are very much similar with differences originating from the fact that they applied it to the π electrons only, and they have used a much smaller width for the steplike charge density distributions. They also have a double-peaked structure for a single-shell fullerene, with a higher intensity for the lower-energy peak; the distance between the two peaks is also decreasing with increasing shell number, although with a much less amount compared to our results for the nanotubes, and up to 40 shells their peaks remain separated. The largest peaks also correspond to the innermost C_{60} molecule, but the next shell's contributions are not as screened as in the case of nanotubes. In the case of the onions, there is no way to vary the radius of the innermost shell, it is always the C_{60} molecule.

In the case of the nanotubes the majority of the theoretical papers treat the π electrons only,[17–19,21,22,24] therefore we cannot compare our results with them for the $\sigma+\pi$ electrons. Huaxiang *et al.*[23] calculated the imaginary part of the dielectric function for the $\sigma+\pi$ electrons for two types of single-shell nanotubes, but for polarization vectors parallel to the tubule axis, while in our calculations it was perpendicular to it. Nevertheless they have the main peak of $\mathrm{Im}\epsilon(\omega)$, at 15.5 eV, and two other peaks at 9.0 eV and 20.0 eV for both kinds of tubules. These are to be compared with the polarizability in our calculations (Figs. 3, 4). Our $\mathrm{Im}\alpha(\omega)$ has a double-peak character with peak positions depending on the diameter and somewhat on the width of the potential well, the closest is the (7,0) tubule to the results of Huaxiang *et al.*[23] The reason for the presence of more peaks in Huaxiang *et al.* may be that they calculated the full spectrum, involving the single-particle excitations too, and our calculation contains only the collective contributions. In the detailed calculations of Yannouleas *et al.*,[25,26] only the frequencies for the collective modes of a nanotube with zero momentum transfer ($q=0$) and with angular momentum $m=1$ can be compared with our dipole polarizability $\alpha(\omega)$. Their results for multishell tubules is based on a model where each shell is supposed to be a two-dimensional cylindrical surface of zero width. In this model only the low-energy tangential mode is active, therefore, for each shell number N, they got exactly N eigenfrequencies. The oscillator strength is the largest for the top level eigenfrequency and this can be compared to the lower-energy peak position of our $\mathrm{Im}\alpha(\omega)$ curves. For $N=1$ and tube radius $R_0\sim 1.69$ nm they got the eigenfrequency at about 6.9 eV [see Fig. 3(a) of Ref. 25], which is favorable comparable to our value of ~ 7.5 eV (Figs. 4, 11) for the tubule (45,0) with a similar radius. By increasing the shell number this peak position, which is the top level of the frequency band, tends to ~ 18 eV in the Yannouleas calculations, and to ~ 18.7 eV in our calculations. There is, however, a discrepancy, the zero momentum transfer ($q=0$) values of the top level frequency for large N values strongly depends on the innermost radius [see Fig. 3(b) of Ref. 25 and Figs. 1(a) and 3 of Ref. 26], while it tends to the same value in our case (Fig. 11). For nonzero momentum transfer this discrepancy quickly disappears.

In summary, plasma oscillations of a cylindrical electron system was investigated in this paper. The main results are the following.

The theory of Mukhopadhyay and Lundqvist[27–29] for the collective oscillations of an inhomogeneous electron system is specified for cylindrical charge distributions. A rectangular potential well model was introduced to calculate the charge density of single-shell nanotubes. The single-particle spectrum exhibits an interesting quasi-one-dimensional character with singularities in the density of states.

In the case of single-shell nanotubes the imaginary part of the dipole polarizabilty shows a double-peaked character.

The peak positions are at 17 and 22 eV for the tubule (7,0) with the smallest radius $R=0.274$ nm. With an increasing radius the peaks tend to separate from each other; the peak at low energy shifts to a lower energy, and the one at high energy to a higher energy (see Fig. 4).

ACKNOWLEDGMENTS

Financial support from the Hungarian Grant OTKA No. 2783/93 is gratefully acknowledged. The author is indebted to his colleagues L. Udvardy, I. Varga, and J. Pipek for their advice on the computer work.

[1] S. Iijima, Nature (London) **354**, 56 (1991).
[2] T.W. Ebbesen and P.M. Ajayan, Nature (London) **358**, 220 (1992).
[3] S. Iijima, P.M. Ajayan, and T. Ichihashi, Phys. Rev. Lett. **69**, 3100 (1992); P.M. Ajayan and S. IIjima, Nature (London) **361**, 333 (1993).
[4] S. Iijima, Y. Ichibashi, Nature (London) **363**, 603 (1993); D.S. Bethune, C.H. Kiang, M.S. de Vries, G. Gorman, R. Savoy, J. Vazquez, and R. Beyers, *ibid.* **363**, 605 (1993); Y. Saito, M. Okuda, N. Fujimoto, T. Yosgikawa, M. Tomita, and T. Hayashi, Jpn. J. Appl. Phys. **33**, L526 (1994); S. Seraphin, J. Electrochem. Soc. **142**, 290 (1995); N. Hatta and K. Murata, Chem. Phys. Lett. **217**, 398 (1994); C.H. Kiang, W.A. Goddard III, R. Beyers, J.R. Salem, and D.S. Bethune, J. Phys. Chem. **98**, 6612 (1994).
[5] M.S. Dresselhaus and G. Dresselhaus, Phys. Rev. B **45**, 6234 (1992); R. Saito, M. Fujita, G. Dresselhaus, and M.S. Dresselhaus, *ibid.* **46**, 1804 (1992); M.S. Dresselhaus, G. Dresselhaus, and R. Saito, Solid State Commun. **84**, 201 (1992).
[6] N. Hamada, S. Sawada, and A. Oshiyama, Phys. Rev. Lett. **68**, 1579 (1992).
[7] J.W. Mintmire, B.I. Dunlap, and C.T. White, Phys. Rev. Lett. **68**, 631 (1992); J.W. Mintmire, D.H. Robertson, and C.T. White, J. Phys. Chem. Solids **54**, 1835 (1993).
[8] C.T. White, D.H. Robertson, and J.W. Mintmire, Phys. Rev. B **47**, 5485 (1993).
[9] H. Yorikawa and S. Muramatsu, Phys. Rev. B **50**, 12 203 (1994); Solid State Commun. **94**, 435 (1995); Phys. Rev. B **52**, 2723 (1995); Solid State Commun. **97**, 115 (1996).
[10] X. Blase, L.X. Benedict, E.L. Shirley, and S.G. Louie, Phys. Rev. Lett. **72**, 1878 (1994).
[11] J.-C. Charlier, X. Gonze, and J.-P. Michenaud, Europhys. Lett. **29**, 43 (1995).
[12] J.-C. Charlier and J.-P. Michenaud, Phys. Rev. Lett. **70**, 1858 (1993).
[13] Ph. Lambin, J.-C. Charlier, and J.-P. Michenaud, in *Progress in Fullerene Research*, Proceedings of the International Winterschool on Electronic Properties of Novel Materials, Kirchberg, Tyrol, Austria, 1994, edited by H. Kuzmany, J. Fink, M. Mehring, and S. Roth (World Scientific, Singapore, 1994), p. 130.
[14] R. Kuzuo, M. Terauchi, and M. Tanaka, Jpn. J. Appl. Phys. **31**, L1484 (1992).
[15] P.M. Ajayan, S. Iijima, and T. Ichihashi, Phys. Rev. B **47**, 6859 (1993).
[16] L.A. Bursil, P.A. Stadelmann, J.L. Peng, and S. Prawer, Phys. Rev. B **49**, 2882 (1994).
[17] M.F. Lin and K.W.-K. Shung, Phys. Rev. B **47**, 6617 (1993).
[18] M.F. Lin and K.W.-K. Shung, Phys. Rev. B **50**, 17 744 (1994).
[19] M.F. Lin, D.S. Chuu, C.S. Huang, Y.K. Lin, and K.W.-K. Shung, Phys. Rev. B **53**, 15 493 (1996).
[20] L.G. Johnson and G. Dresselhaus, Phys. Rev. B **7**, 2275 (1973).
[21] O. Sato, Y. Tanaka, M. Kobayashi, and A. Hasegawa, Phys. Rev. B **48**, 1947 (1993).
[22] P. Longe and S.M. Bose, Phys. Rev. B **48**, 18 239 (1993).
[23] F. Huaxiang, Y. Ling, and X. Xide, Solid State Commun. **91**, 191 (1994).
[24] P.S. Davids, L. Wang, A. Saxena, and A.R. Bishop, Phys. Rev. B **49**, 5682 (1994); **51**, 4557 (1995).
[25] C. Yannouleas, E.N. Bogachek, and U. Landman, Phys. Rev. B **50** , 7977 (1994).
[26] C. Yannouleas, E.N. Bogachek, and U. Landman, Phys. Rev. B **53**, 10 225 (1996).
[27] G. Mukhopadhyay and S. Lundqvist, Il Nuovo Cimento **27B**, 1 (1975).
[28] G. Mukhopadhyay and S. Lundqvist, J. Phys. B **12**, 1297 (1979).
[29] S. Lundqvist, in *Theory of the Inhomogeneous Electron Gas*, edited by S. Lunqvist and N.H. March (Plenum Press, New York, 1983), p. 149.
[30] D. Östling, P. Apell, and A. Rosen, Europhys. Lett. **21**, 539 (1993).
[31] B. Vasvári, Z. Phys. B **100**, 223 (1996).
[32] J.D. Jackson, *Classical Electrodynamics*, 2nd ed. (Wiley, New York, 1975), Sec. 3.11.
[33] Ph. Lambin, A.A. Lucas, and J.-P. Vigneron, Phys. Rev. B **46**, 1794 (1992).
[34] P. Apell, D. Östling, and G. Mukhopadhyay, Solid State Commun. **87**, 219 (1993).